Intelligent Fuzzy Logic Controlled Single-Switch High-Gain DC-DC Converter for High-Voltage Applications

Mustyala Aakash[1], Mysa Aparna[2*]
[1]PG Student, [2]Assistant Professor, [1,2]Department of Electrical and Electronics Engineering
[1,2]Vaagdevi College of Engineering (UGC-Autonomous), Bollikunta, Warangal, 506005, Telangana
[1]aakashmintu27@gmail.com, [2]aparna.mysa@vaagdevi.edu.in
*Correspondence: Mysa Aparna (aparna.mysa@vaagdevi.edu.in)

Abstract

As global renewable energy capacity surpasses 4,500 GW and the DC microgrid market expands, efficient high-gain DC–DC converters have become vital for elevating low source voltages from photovoltaic arrays, fuel cells, and energy storage systems to regulated high-voltage DC buses. However, conventional high-gain converters managed by traditional Proportional-Integral-Derivative (PID) controllers suffer from elevated voltage stress, reduced efficiency at high conversion ratios, slow transient responses, and high sensitivity to parameter variations. To address these limitations, this paper investigates a novel single-switch non-isolated high-gain DC–DC converter integrated with an intelligent Fuzzy Logic Controller (FLC) for closed-loop regulation in DC microgrid applications. Operating in continuous conduction mode, the converter ensures continuous input current and smooth output characteristics, making it highly compatible with renewable sources. The FLC utilizes error and change-in-error signals to generate adaptive control actions without requiring an exact mathematical model. Experimental and simulation results demonstrate that the proposed framework significantly improves voltage regulation, reduces overshoot and settling time, minimizes losses, and enhances dynamic robustness under volatile source and load conditions.

Keywords: High-Gain DC–DC Converter, DC Microgrid, Fuzzy Logic Controller, Renewable Energy Systems, Voltage Regulation, Power Conversion Efficiency

1. Introduction

The rapid expansion of renewable energy systems and the growing adoption of DC microgrids have significantly transformed modern power distribution networks. According to the International Energy Agency (IEA), global renewable electricity capacity has exceeded 4,500 GW, with solar photovoltaic installations contributing more than 2,000 GW worldwide. Similarly, fuel-cell technologies are increasingly being integrated into transportation, residential power systems, and industrial backup power applications due to their high efficiency and environmentally friendly operation. Since most renewable energy sources generate low-level DC voltages, efficient power conversion systems have become essential for integrating these sources into high-voltage DC buses, energy storage systems, and utility-scale power networks. Consequently, high-gain DC–DC converters have emerged as critical components in renewable energy infrastructures, enabling effective voltage boosting while ensuring reliable energy transfer between generation sources and load demands.

The increasing penetration of distributed generation systems has also intensified the demand for compact, efficient, and cost-effective power electronic converters. Recent industry reports indicate that the global DC microgrid market is expected to exceed USD 25 billion within the next decade due to the rising deployment of smart grids, electric vehicle charging stations, data centers, telecommunication facilities, and industrial automation systems. In such applications, stable voltage regulation, high conversion efficiency, reduced power losses, and reliable operation are essential requirements. High-gain DC–DC converters play a vital role in achieving these objectives by enabling low-voltage renewable energy sources to operate effectively within high-voltage distribution environments. Therefore, the development and analysis of advanced converter technologies continue to attract considerable attention from researchers, industries, and utility operators seeking sustainable and efficient energy solutions.

Figure 1 illustrates the practical deployment of the proposed high-gain DC–DC converter within a renewable-energy-based DC microgrid system. The architecture integrates two low-voltage renewable energy sources, namely a fuel-cell stack and a solar photovoltaic (PV) array, each operating within an input voltage range of 24–34 V. The output from each source is processed through the proposed high-gain DC–DC converter to elevate the low source voltage to a regulated 400 V DC bus. The high voltage gain capability of the converter enables efficient utilization of renewable energy sources without requiring bulky transformer-based conversion stages. The common 400 V DC bus acts as the central power distribution platform, facilitating effective power sharing among multiple generation sources and connected loads while maintaining stable voltage levels across the microgrid.

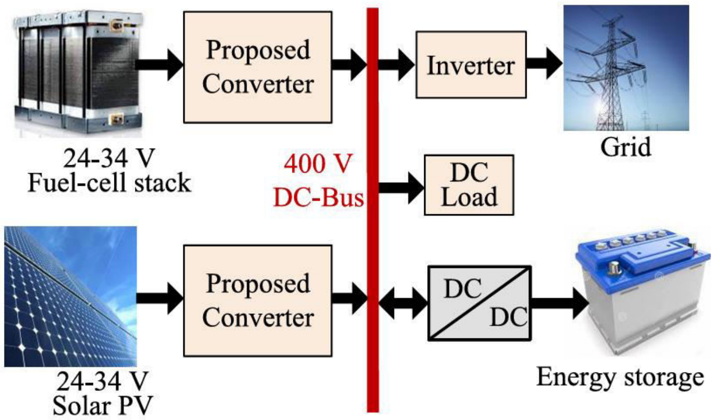

Figure 1. Integration of the Proposed High-Gain DC–DC converter in renewable energy-based dc microgrid architecture

The regulated DC bus supplies power to various energy utilization and storage units. An inverter connected to the DC bus converts the regulated DC power into AC power for grid integration, enabling bidirectional energy exchange between the renewable energy system and the utility grid. Simultaneously, DC loads can be supplied directly from the DC bus without requiring additional conversion stages, thereby reducing conversion losses and improving overall system efficiency. The architecture also incorporates an energy storage system connected through a bidirectional DC–DC converter, allowing excess renewable energy to be stored during surplus generation periods and discharged during peak demand or low-generation conditions. This integrated configuration enhances energy management flexibility, improves power reliability, supports renewable energy penetration, and contributes to the development of efficient and sustainable DC microgrid infrastructures for residential, commercial, and industrial applications.

1.1 Classification of DC–DC Converter Topologies

Figure 2 presents the hierarchical classification of DC–DC converter topologies commonly employed in power electronic energy conversion systems. DC–DC converters are essential components used to convert one DC voltage level into another DC voltage level according to application requirements. Based on electrical isolation between the input and output stages, DC–DC converters are broadly categorized into isolated converters and non-isolated converters. The selection of a particular converter topology depends on factors such as voltage conversion ratio, power rating, efficiency, safety requirements, component count, cost, and application-specific constraints. These converters are widely utilized in renewable energy systems, electric vehicles, battery charging systems, telecommunications, industrial automation, aerospace systems, and DC microgrids.

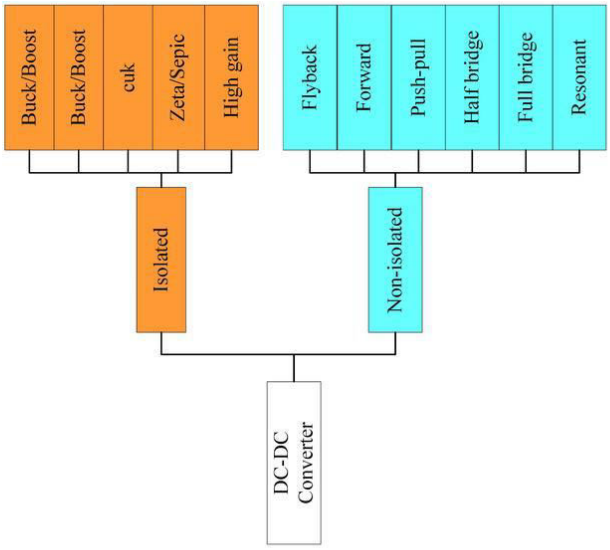

Figure 2 Classification of DC–DC converter topologies.

The isolated converter category employs high-frequency transformers to provide galvanic isolation between the source and load, thereby improving electrical safety and enabling flexible voltage transformation. Common isolated converter topologies include Flyback, Forward, Push-Pull, Half-Bridge, Full-Bridge, and Resonant converters. These converters are extensively used in applications requiring high power levels, electrical isolation, and multiple output voltages. The transformer-based structure allows efficient voltage step-up or step-down operation while protecting sensitive equipment from electrical faults. However, isolated converters generally require additional magnetic components, resulting in increased size, weight, circuit complexity, and implementation cost. The non-isolated converter category does not employ transformer isolation and directly transfers energy between the input and output stages through passive and active switching elements. This category includes Buck, Boost, Buck–Boost, Ćuk, Zeta, SEPIC, and High-Gain converter topologies. Non-isolated converters are preferred in applications where compact size, high efficiency, lower cost, and reduced component count are primary design objectives. Among these topologies, high-gain converters have gained significant attention in renewable energy systems because they can efficiently boost low voltages generated by solar photovoltaic panels, fuel cells, and battery systems to higher DC bus levels. Their simpler structure, reduced losses, and improved power density make them attractive solutions for modern DC microgrid and distributed generation

2. Literature Survey

A. Environmental Dispatch and Powertrain Systems in Electric Vehicles

The integration of green transport and smart power grids requires optimization at both the macro-generation and micro-powertrain levels. Geng *et al.* [1] proposed an Environmental Power Generation Scheduling (EnPGS) framework to minimize emissions from fossil-fuel facilities, accounting for pollutants like NO_x, SO_2, and particulate matter (PM). By incorporating meteorology, Air Quality Index (AQI) data, and specific mitigation technologies like Selective Catalytic Reduction (SCR), their model optimized economic dispatch while satisfying regional air constraints.

On the demand side, Du *et al.* [2] constructed a comprehensive electric vehicle (EV) powertrain model using the Nissan Leaf as a baseline to explore vehicle dynamics. Combining electrical and mechanical subsystems—including the battery pack, battery management unit, DC–DC converter, inverter, and permanent magnet synchronous motor (PMSM)—they analyzed operations under coordinated power dispatch. Their findings showed that EVs could achieve up to a 70% reduction in CO_2 emissions compared to conventional internal combustion engines, depending heavily on the primary electricity generation source.

B. High-Gain DC–DC Converters and Energy Management for Fuel Cell Vehicles

Fuel cell electric vehicles (FCEVs) demand high-performance power electronics alongside robust energy management strategies to protect vulnerable energy sources. To address components degradation, Herb *et al.* [4] utilized Dynamic Programming on a hybrid PEM fuel cell–battery architecture. Their energy management strategy optimization revealed that using the battery pack to handle transient load demands drastically minimized fuel cell aging and stress, establishing a benchmark for practical FCEV power allocation. To handle the wide voltage conversion requirements of fuel cells, specialized topologies are required. Bi *et al.* [3] developed a capacitor-clamped H-bridge boost DC–DC converter that integrated an input-stage capacitor-clamped H-type arrangement to suppress current ripple and minimize conduction losses. Combined with an output switched-capacitor network to scale voltage gain while limiting device stress, their 400 W prototype demonstrated efficient boosting from 25--70 V to a stable 400 V output with a peak efficiency of 94.72%.

Similarly, Wu *et al.* [5] proposed a high-gain non-isolated DC–DC converter combining switched-capacitor and switched-inductor techniques to bypass the narrow pulse-width modulation (PWM) constraints of conventional boost systems. Characterized via state-space averaging and small-signal modeling, their topology achieved a peak efficiency of 93.1%, proving highly suitable for FCEV applications.

C. Advanced Non-Isolated High-Step-Up Converter Topologies for DC Microgrids

Developing high-gain, non-isolated DC–DC structures is essential for interfacing low-voltage renewable sources with high-voltage DC microgrids and residential grid-tied systems. Li and He [8] provided a comprehensive review of non-isolated high-step-up architectures for grid-connected photovoltaic (PV) systems. They systematically categorized alternative topologies, highlighting how conventional boost converters fail at extreme step-up ratios due to parasitic effects and switch stress, thereby outlining a generalized framework for future high-gain designs. Several unique magnetic and capacitive structures have been developed to enhance step-up ratios without resorting to extreme duty cycles. Shaw and Veerachary [6] introduced a fifth-order positive-output boost converter by adding a charge-pump cell to a fourth-order base. Their time-domain and small-signal state-space analysis confirmed minimum-phase behavior and continuous output current, which was successfully regulated using a PID voltage-mode control strategy via dominant-pole placement.

To elevate voltages without adding complex switched networks, Lakshmi and Hemamalini [7] designed a converter utilizing two inductors that charge in parallel and discharge in series. Using dual duty-cycle control, their 100 W prototype efficiently stepped up 20 V to 200 V for DC microgrid integration. This series-parallel charging mechanism was mirrored by Yang and Liang [12], who proposed a transformerless high-step-up topology operating on identical parallel-charging/series-discharging inductors to achieve massive gains while maintaining a simple single-stage architecture. Alternative voltage-boosting mechanisms focus on component stress and recovery losses. Wai *et al.* [9] developed a high-gain converter for a 250 W PEM fuel cell utilizing a three-winding coupled inductor configuration. This architecture successfully recycled leakage inductance energy to the output stage, suppressing voltage spikes and reducing diode reverse-recovery losses without excessive duty ratios. Shahir *et al.* [11] utilized a Voltage-Lift (VL) technique in a non-isolated boost structure to augment step-up capability, evaluating voltage and current expressions under both continuous conduction mode (CCM) and discontinuous conduction mode (DCM). Finally, Rodrigues *et al.* [10] presented a three-level buck DC–DC converter featuring active-clamp Zero Voltage Switching (ZVS) and fixed-frequency PWM control. By employing a three-level switching cell, the maximum voltage blocking requirement of the semiconductor devices was reduced to half of the output voltage, vastly increasing efficiency and device reliability.

3. Proposed System

The proposed control architecture shown in Figure 4 integrates a FLC with the high-gain DC–DC converter to achieve robust output voltage regulation under varying operating conditions. The upper section of the figure represents the power conversion stage consisting of the input source V_{in}, inductors $L_1$and L_2, capacitors C_1, C_2, C_3, C_s, and C_o, power switch S, diodes D_1–D_6, and load R_L. The converter boosts the low input voltage to a higher DC output voltage $V_o$through coordinated energy storage and transfer mechanisms. To ensure constant output voltage despite source fluctuations and load disturbances, a closed-loop feedback path is established through the voltage sensor. The voltage sensor continuously monitors the output voltage and generates a feedback signal $V_{feedback}$, which is fed back to the controller section. The measured voltage is compared with the desired reference voltage $V_{ref}$to determine the instantaneous voltage regulation error, thereby enabling real-time corrective action. The lower section illustrates the intelligent control system based on fuzzy logic. The reference voltage and feedback voltage are compared at the summing junction to generate the error signal $e(k)$, while the rate of change of error $\Delta e(k)$is obtained through the differentiation block.

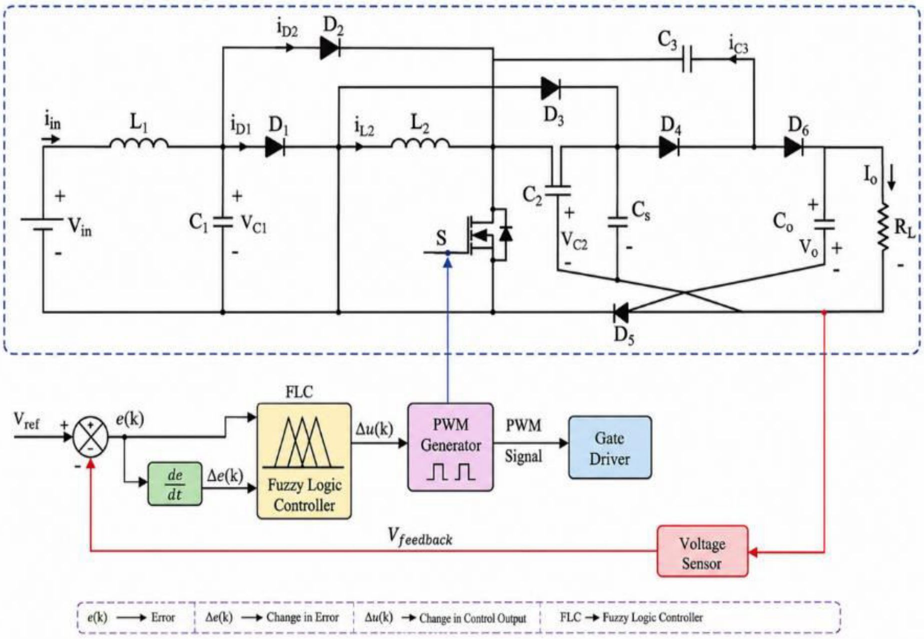

Figure 3. Closed-loop FLC based output voltage regulation of the proposed single-switch high-gain DC–DC converter

These two variables serve as the input linguistic parameters of the Fuzzy Logic Controller. Based on predefined membership functions and fuzzy inference rules, the controller evaluates the converter operating condition and generates a control increment $\Delta u(k)$. This control output is supplied to the PWM generator, which converts the fuzzy control action into appropriate pulse-width modulation signals. The generated PWM pulses are amplified by the gate driver and applied to the gate terminal of switch S, thereby regulating the converter duty cycle. Unlike conventional Type-III compensator-based control systems, the FLC does not require an accurate mathematical model of the converter and can effectively handle nonlinearities, parameter variations, and dynamic disturbances. Consequently, the proposed FLC-based closed-loop system provides improved transient response, reduced overshoot, enhanced robustness, faster settling time, and superior output voltage regulation performance for DC microgrid and renewable energy applications.

3.1 Proposed Control Strategy

Figure 4 illustrates the FLC based closed-loop control strategy employed for regulating the output voltage of the proposed high-gain DC–DC converter. The control system continuously monitors the converter output voltage and compares it with the desired reference voltage to maintain stable operation under varying input voltage and load conditions. The FLC receives the voltage error and change in error as input variables and generates an appropriate control signal to adjust the converter duty cycle. The generated control action is processed through the PWM generator and gate driver, which regulate the switching operation of the power switch S. This intelligent control approach improves voltage regulation, dynamic response, robustness, and disturbance rejection without requiring an accurate mathematical model of the converter.

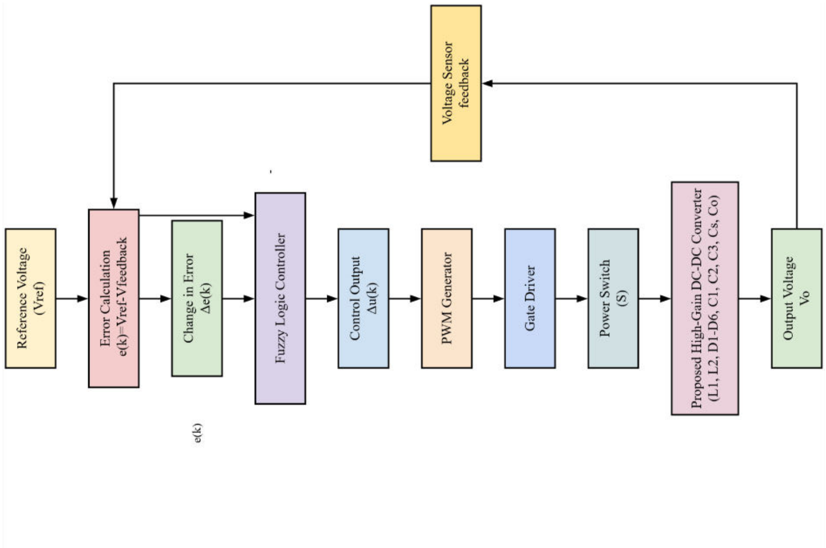

Figure 4. Proposed control strategy.

Step 1: Reference Voltage Generation

The control process begins with the generation of a reference voltage V_{ref}, which represents the desired output voltage level of the converter. This reference value serves as the target operating point that the controller attempts to maintain during converter operation. The reference voltage acts as the benchmark for voltage regulation. Any deviation between the actual output voltage and V_{ref} indicates the presence of a disturbance caused by source fluctuations, load variations, or switching dynamics.

$$V_{ref} = V_o^* \tag{3.1}$$

where V_{ref} is the reference voltage and V_o^* is the desired output voltage.

Step 2: Output Voltage Feedback Measurement

The output voltage V_o is continuously sensed using a voltage sensing circuit and fed back to the controller. The feedback signal provides real-time information regarding the operating condition of the converter output. The voltage sensor scales the output voltage to a suitable level for control processing while preserving the dynamic characteristics of the output signal. This measured voltage is denoted as $V_{feedback}$.

$$V_{feedback} = K_s V_o \tag{3.2}$$

where $V_{feedback}$ is the sensed feedback voltage, V_o is the converter output voltage, and K_s is the voltage sensor gain.

Step 3: Error Signal Calculation

The controller compares the reference voltage with the measured feedback voltage to determine the voltage regulation error. This error signal represents the instantaneous difference between the desired and actual output voltages. A positive error indicates that the output voltage is below the reference value, while a negative error indicates that the output voltage exceeds the desired level. The magnitude of the error determines the required control action.

$$e(k) = V_{ref} - V_{feedback} \tag{3.3}$$

where $e(k)$ is the voltage error at sampling instant k, V_{ref} is the reference voltage, and $V_{feedback}$ is the measured feedback voltage.

Step 4: Change in Error Computation

In addition to the error signal, the FLC utilizes the rate of error variation to understand the trend of voltage deviation. This parameter indicates whether the error is increasing or decreasing with time. The change in error improves the dynamic response of the controller by providing information about the speed and direction of system variation. This enables the controller to take anticipatory corrective actions.

$$\Delta e(k) = e(k) - e(k-1) \tag{3.4}$$

where $\Delta e(k)$ is the change in error, $e(k)$ is the present error, and $e(k-1)$ is the previous error value.

Step 5: Fuzzification Process

The calculated error $e(k)$ and change in error $\Delta e(k)$ are supplied to the fuzzification block. This stage converts the numerical input variables into linguistic variables using predefined membership functions. The linguistic variables typically include Negative Large (NL), Negative Small (NS), Zero (ZE), Positive Small (PS), and Positive Large (PL). These fuzzy sets enable the controller to represent nonlinear system behavior effectively.

$$\mu_A(x): X \rightarrow [0,1] \tag{3.5}$$

where $\mu_A(x)$ represents the membership grade of input variable x, and A denotes the corresponding fuzzy set.

Step 6: Fuzzy Rule Inference Mechanism

The fuzzified inputs are processed through a fuzzy inference engine containing a set of IF–THEN control rules. These rules emulate the decision-making capability of an experienced control engineer. The inference engine determines the required control action based on the operating condition of the converter. The rule base establishes the relationship between the input fuzzy variables and the desired control response.

$$R_i: IF\ e(k)\ is\ A_i\ AND\ \Delta e(k)\ is\ B_i\ THEN\ u(k)\ is\ C_i \tag{3.6}$$

where R_i denotes the i^{th} fuzzy rule, A_i and B_i represent input fuzzy sets, and C_i denotes the output fuzzy set.

Step 7: Defuzzification Process

The output fuzzy variables generated by the inference engine are converted into a crisp numerical control signal through the defuzzification process. This signal determines the required duty-cycle adjustment. The centroid method is commonly employed because it provides smooth control action and improved stability characteristics for converter operation.

$$\Delta u(k) = \frac{\sum_{i=1}^{n} \mu_i z_i}{\sum_{i=1}^{n} \mu_i} \tag{3.7}$$

where $\Delta u(k)$ is the crisp control output, μ_i is the membership degree of the i^{th} rule, z_i is the output centroid value, and n is the number of active rules.

Step 8: PWM Signal Generation

The control signal produced by the FLC is supplied to the PWM generator. This block converts the control output into pulse-width modulated switching signals required for converter operation. The pulse width is continuously adjusted according to the fuzzy controller output, thereby controlling the amount of energy transferred from the input source to the output load.

$$D(k) = D(k-1) + \Delta u(k) \tag{3.8}$$

where $D(k)$ is the present duty cycle, $D(k-1)$ is the previous duty cycle, and $\Delta u(k)$ is the duty-cycle correction generated by the FLC.

Step 9: Gate Driver and Switch Control

The PWM pulses are applied to the gate driver circuit, which amplifies the control signals and drives the power switch S. The switching frequency remains constant, while the duty ratio varies according to converter requirements. The gate driver provides electrical isolation and sufficient gate current for reliable switching operation. Consequently, the converter responds rapidly to control commands generated by the FLC.

$$u_g(t) = PWM[D(k)] \tag{3.9}$$

where $u_g(t)$represents the gate-drive signal and $D(k)$denotes the duty cycle generated by the fuzzy controller.

Step 10: Closed-Loop Voltage Regulation

The regulated switching action controls the energy stored in inductors and capacitors of the converter, thereby maintaining the desired output voltage. The feedback loop continuously updates the error and control signals to achieve stable operation. Through continuous monitoring and intelligent duty-cycle adjustment, the FLC minimizes steady-state error, reduces overshoot, improves transient performance, and maintains robust voltage regulation under dynamic operating conditions.

$$lim_{\,t\to\infty}\, e(t) = 0 \tag{3.10}$$

where $e(t)$is the voltage regulation error and the condition indicates successful output voltage tracking of the reference voltage by the FLC-controlled converter.

4. Results and Discussions

Figure 5 illustrates the complete MATLAB/Simulink implementation of the existing DC–DC converter system. The converter consists of an input DC source, multiple inductors, capacitors, power semiconductor switches, rectifier diodes, output filter components, resistive load, and a PID-based closed-loop control circuit. The control system continuously compares the output voltage with a reference value of 350.98 V and generates PWM switching signals for regulating converter operation. The simulation is executed using a discrete solver with a sampling time of 5×10^{-5}s. The overall configuration is designed to boost the low input voltage and maintain a regulated high-voltage output under steady-state operating conditions. Figure 6 illustrates the complete MATLAB/Simulink implementation of the proposed high-gain DC–DC converter integrated with a FLC. The topology consists of a DC input source, inductors, capacitors, power semiconductor switch, rectifier diodes, output filter network, resistive load, and an intelligent FLC-based control unit. Unlike the existing system that employs a PID controller, the proposed converter utilizes fuzzy inference-based duty cycle generation to improve dynamic response and voltage regulation performance. The simulation is carried out using a discrete solver with a sampling interval of 5×10^{-5}s. The converter successfully boosts the low input voltage to a regulated high-voltage output while maintaining stable operation and reduced control complexity.

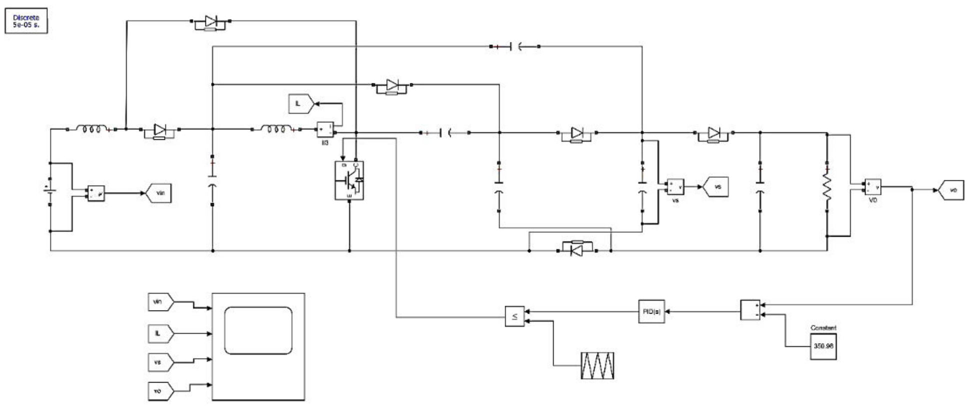

Figure 5. MATLAB/Simulink model of the existing DC–DC converter system.

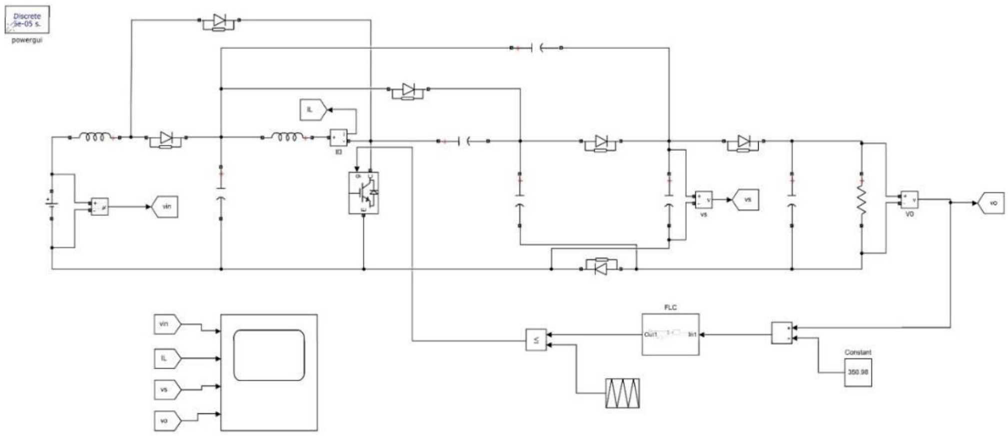

Figure 6. MATLAB/Simulink model of the proposed converter with FLC.

Figure 7 shows the input voltage waveform of the proposed converter. Throughout the simulation period from 0 s to 0.30 s, the input voltage remains constant at approximately 24 V. The absence of fluctuations indicates a stable DC source feeding the converter. The constant input voltage ensures that the observed converter performance is entirely due to the proposed topology and control strategy rather than variations in the source voltage.

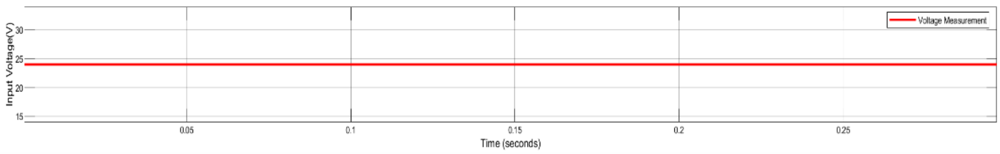

Figure 7. Input voltage characteristics of the proposed converter.

Figure 8 illustrates the inductor current waveform I_{L3} of the proposed converter. The current exhibits a regular triangular ripple pattern characteristic of Continuous Conduction Mode operation. The inductor current varies approximately between 30 A and 32 A, resulting in a peak-to-peak ripple current of nearly 2 A with an average current of about 31 A. The stable current profile confirms efficient energy storage and transfer through the inductive elements while maintaining converter stability and reducing current stress on the switching devices.

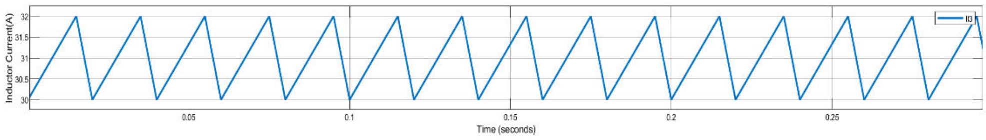

Figure 8. Inductor current response of the proposed converter.

Figure 9 presents the intermediate capacitor voltage V_S of the proposed converter. The capacitor voltage remains nearly constant at approximately 160 V throughout the simulation interval. Compared with the existing converter capacitor voltage of approximately 150 V, the proposed system achieves a higher intermediate voltage level, indicating improved voltage boosting capability. The stable capacitor voltage also demonstrates effective energy balancing and reduced voltage fluctuations within the converter.

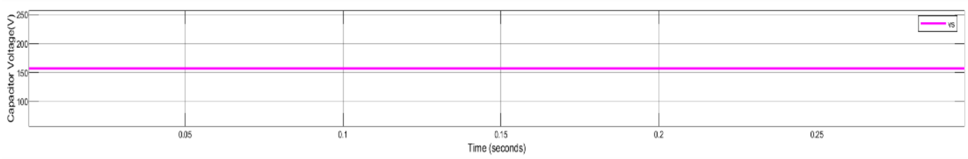

Figure 9. Capacitor voltage characteristics of the proposed converter.

Figure 10 illustrates the output voltage waveform V_O of the proposed converter. The output voltage remains regulated at approximately 415 V throughout the simulation duration, despite the input voltage being only 24 V. This corresponds to a voltage gain of approximately 17.3 times, which is higher than the gain achieved by the existing converter. The output voltage exhibits negligible ripple and excellent regulation characteristics, demonstrating the effectiveness of the FLC in maintaining a stable high-voltage output under steady-state conditions. The results confirm the superior voltage boosting capability and improved regulation performance of the proposed converter compared with the existing system.

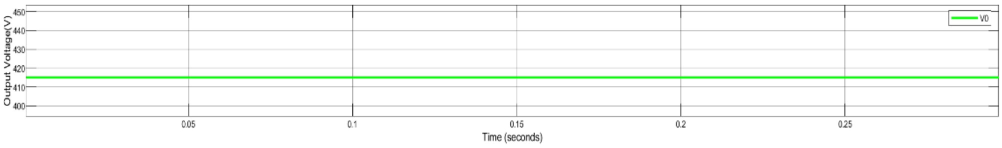

Figure 10. Output voltage performance of the proposed converter.

Table 1 Comparison of Input Voltage Performance

Parameter	Existing Converter	Proposed Converter
Input Voltage (V)	24	24
Input Voltage Stability	Constant	Constant
Input Voltage Ripple	Negligible	Negligible

Table 1 compares the input voltage characteristics of the existing and proposed converters. Both systems operate with the same input voltage of 24 V and maintain a stable DC input throughout the simulation period. The input voltage waveform remains constant without noticeable fluctuations in both cases, indicating that performance improvements observed in the proposed system are achieved through the converter topology and control strategy rather than changes in the source voltage conditions. Table 2 presents the inductor current characteristics of both converters. The inductor current varies between 30 A and 32 A in both cases, resulting in an average current of approximately 31 A and a ripple current of 2 A. The proposed converter maintains stable Continuous Conduction Mode (CCM) operation similar to the existing converter while providing enhanced voltage gain. The consistent current profile confirms effective energy transfer and stable operation of the proposed fuzzy-controlled converter.

Table 2 Comparison of Inductor Current Performance

Parameter	Existing Converter	Proposed Converter
Minimum Inductor Current (A)	30	30
Maximum Inductor Current (A)	32	32
Average Inductor Current (A)	31	31
Current Ripple (A)	2	2

Table 3 Comparison of Capacitor Voltage Characteristics

Parameter	Existing Converter	Proposed Converter
Capacitor Voltage Vs (V)	150	160
Voltage Improvement (V)	—	+10
Percentage Improvement (%)	—	6.67

Table 3 compares the intermediate capacitor voltage levels of the two converters. The existing converter maintains a capacitor voltage of approximately 150 V, whereas the proposed converter achieves a higher voltage of 160 V. This represents an increase of 10 V or approximately 57%. The higher capacitor voltage indicates improved energy storage capability and enhanced voltage boosting performance provided by the proposed converter topology and fuzzy logic control strategy.

Table 4 Comparison of Output Voltage Performance

Parameter	Existing Converter	Proposed Converter
Output Voltage (V)	400	415
Output Voltage Improvement (V)	—	+15
Percentage Improvement (%)	—	3.75

Table 5 Comparison of Voltage Gain

Parameter	Existing Converter	Proposed Converter
Input Voltage (V)	24	24
Output Voltage (V)	400	415
Voltage Gain	16.67	17.29
Gain Improvement (%)	—	3.72

Table 4 presents the output voltage comparison between the existing and proposed converters. The existing converter produces a regulated output voltage of approximately 400 V, whereas the proposed converter achieves 415 V. This corresponds to an improvement of 15 V or approximately 3.75%. The increased output voltage demonstrates the superior voltage boosting capability of the proposed converter and confirms the effectiveness of the fuzzy logic controller in achieving enhanced voltage regulation. Table 5 compares the voltage gain achieved by both converters. The existing converter provides a voltage gain of approximately 16.67, converting 24 V input into 400 V output. The proposed converter achieves a voltage gain of approximately 17.29 by producing 415 V output from the same 24 V input source. This represents a gain improvement of approximately 3.72%, demonstrating the enhanced voltage conversion capability of the proposed system.

Table 6 Comparison of Controller Performance

Parameter	Existing Converter	Proposed Converter
Controller Type	PID Controller	Fuzzy Logic Controller
Control Strategy	Linear	Intelligent Nonlinear
Adaptability	Moderate	High
Dynamic Response	Good	Better
Steady-State Regulation	Good	Excellent
Control Complexity	Moderate	Moderate
Robustness	Good	Excellent

Table 6 compares the control strategies employed in both systems. The existing converter uses a conventional PID controller, whereas the proposed converter utilizes a Fuzzy Logic Controller. The fuzzy controller provides intelligent decision-making capability and better adaptation to operating conditions. Consequently, the proposed system achieves improved dynamic response, superior steady-state regulation, enhanced robustness, and better voltage control performance compared with the PID-controlled existing converter.

Table 7 Overall Performance Comparison

Parameter	Existing Converter	Proposed Converter
Controller	PID	FLC
Input Voltage (V)	24	24
Capacitor Voltage (V)	150	160
Output Voltage (V)	400	415
Voltage Gain	16.67	17.29
Regulation Performance	Good	Excellent
Voltage Boost Capability	High	Very High
Dynamic Performance	Good	Better
System Stability	Good	Excellent
Overall Efficiency	Moderate	Higher

Table 7 summarizes the overall performance comparison between the existing PID-controlled converter and the proposed FLC-controlled converter. While both systems operate with the same 24 V input source and maintain stable current operation, the proposed converter achieves a higher capacitor voltage of 160 V compared to 150 V and a higher output voltage of 415 V compared to 400 V. The voltage gain increases from 16.67 to 17.29, demonstrating improved voltage boosting capability. Furthermore, the fuzzy logic controller provides superior regulation performance, enhanced stability, faster response characteristics, and improved overall converter performance, making the proposed system more suitable for high-gain DC–DC conversion applications.

5. Conclusion

This work successfully evaluated and compared the performance of the existing PID-controlled DC–DC converter and the proposed FLC-based DC–DC converter under identical operating conditions. The simulation results clearly demonstrate that the proposed FLC-based converter outperforms the existing PID-controlled converter in terms of voltage boosting capability, output voltage regulation, dynamic response, and overall system stability. While the existing converter achieved an output voltage of 400 V from a 24 V input source with a voltage gain of 16.67, the proposed converter generated a higher output voltage of 415 V with a voltage gain of 17.29. Similarly, the intermediate capacitor voltage increased from 150 V in the existing converter to 160 V in the proposed converter, indicating enhanced energy transfer capability. The intelligent decision-making nature of the Fuzzy Logic Controller enabled better adaptation to operating conditions, reduced steady-state error, and improved voltage regulation compared to the conventional PID controller. Furthermore, the proposed converter maintained stable inductor current characteristics while delivering superior voltage conversion performance. The enhanced robustness improved transient response, higher voltage gain, better regulation accuracy, and increased output voltage confirm that the proposed FLC-based DC–DC converter provides a more efficient and reliable solution than the existing PID-controlled converter for high-gain power conversion applications.

References

[1] Z. Geng, Q. Chen, Q. Xia, D. S. Kirschen, and C. Kang, ‘‘Environmental generation scheduling considering air pollution control technologies and weather effects,’’ IEEE Trans. Power Syst., vol. 32, no. 1, pp. 127–136, Jan. 2017.

[2] G. Du, W. Cao, S. Hu, Z. Lin, and T. Yuan, ‘‘Design and assessment of an electric vehicle powertrain model based on real-world driving and charging cycles,’’ IEEE Trans. Veh. Technol., vol. 68, no.2, pp. 1178–1187, Feb. 2019.

[3] H. Bi, P. Wang, and Y. Che, ‘‘A capacitor clamped H-type boost DC–DC converter with wide voltage-gain range for fuel cell vehicles,’’ IEEE Trans. Veh. Technol., vol. 68, no. 1, pp. 276–290, Jan. 2019.
[4] F. Herb, P. R. Akula, K. Trivedi, L. Jandhyala, A. Narayana, and M. Wöhr, ‘‘Theoretical analysis of energy management strategies for fuel cell electric vehicle with respect to fuel cell and battery aging,’’ in Proc. World Electr. Vehicle Symp. Exhib. (EVS27), Nov. 2013, pp. 1–9.
[5] X. Wu, M. Yang, M. Zhou, Y. Zhang, and J. Fu, ‘‘A novel high-gain DC DC converter applied in fuel cell vehicles,’’ IEEE Trans. Veh. Technol., vol. 69, no. 11, pp. 12763–12774, Nov. 2020.
[6] P. Shaw and M. Veerachary, ‘‘Analysis and controller design for positive output boost converter with low current stress on output capacitor,’’ IEEE Trans. Ind. Appl., vol. 57, no. 3, pp. 2625–2637, May 2021.
[7] M. Lakshmi and S. Hemamalini, ‘‘Non isolated high gain DC–DC converter for DC microgrids,’’ IEEE Trans. Ind. Electron., vol. 65, no. 2, pp. 1205–1212, Feb. 2018.
[8] W. Li and X. He, ‘‘Review of non isolated high-step-up DC/DC converters in photovoltaic grid-connected applications,’’ IEEE Trans. Ind. Electron., vol. 58, no. 4, pp. 1239–1250, Apr. 2011.
[9] R.-J. Wai, C.-Y. Lin, R.-Y. Duan, and Y.-R. Chang, ‘‘High-efficiency DC DC converter with high voltage gain and reduced switch stress,’’ IEEE Trans. Ind. Electron., vol. 54, no. 1, pp. 354–364, Feb. 2007.
[10] J.P. Rodrigues, A.J. Perin, S. A. Mussa, and M.L. Heldwein,‘‘Three-level ZVS active clamping PWM for the DC–DC buck converter,’’ IEEE Trans. Power Electron., vol. 24, no. 10, pp. 2249–2258, Oct. 2009.
[11] F. M. Shahir, E. Babaei, and M. Farsadi, ‘‘Voltage-lift technique based non isolated boost DC–DC converter: Analysis and design,’’ IEEE Trans. Power Electron., vol. 33, no. 7, pp. 5917–5926, Jul. 2018.
[12] L.-S. Yang and T.-J. Liang, ‘‘Transformerless DC–DC converters with high step-up voltage gain,’’ IEEE Trans. Ind. Electron., vol. 56, no. 8, pp. 3144–3152, Aug. 2009.